ACS APPLIED MATERIALS & INTERFACES

Research Article

www.acsami.org

Two-in-One Strategy for Effective Enrichment of Phosphopeptides Using Magnetic Mesoporous γ-Fe_2O_3 Nanocrystal Clusters

Yuting Zhang,[†,§] Lulu Li,[‡,§] Wanfu Ma,[†] Ying Zhang,[‡] Meng Yu,[†] Jia Guo,[†] Haojie Lu,*[,‡] and Changchun Wang*[,†]

[†]State Key Laboratory of Molecular Engineering of Polymers and Department of Macromolecular Science, Laboratory of Advanced Materials, Fudan University, Shanghai 200433, China

[‡]Department of Chemistry and Institutes of Biomedical Sciences, Fudan University, Shanghai 200032, People's Republic of China

Supporting Information

ABSTRACT: Designed with a two-in-one strategy, the magnetic mesoporous γ-Fe_2O_3 nanocrystal clusters (m-γ-Fe_2O_3) have been successfully prepared for integrating the functions of effective enrichment and quick separation of phosphopeptides into a single architecture. First, the mesoporous Fe_3O_4 nanocrystal clusters (mFe_3O_4) were synthesized by solvothermal reaction and then were subjected to calcination in air to form m-γ-Fe_2O_3. The obtained m-γ-Fe_2O_3 have spherical morphology with uniform particle size of about 200 nm and mesoporous structure with the pore diameter of about 9.7 nm; the surface area is as large as 117.8 m^2/g, and the pore volume is 0.34 cm^3/g. The m-γ-Fe_2O_3 possessed very high magnetic responsiveness (Ms = 78.8 emu/g, magnetic separation time from solution is less than 5 s) and were used for the selective enrichment of phosphopeptides for the first time. The experimental results demonstrated that the m-γ-Fe_2O_3 possessed high selectivity for phosphopeptides at a low molar ratio of phosphopeptides/nonphosphopeptides (1:100), high sensitivity (the detection limit was at the fmol level), high enrichment recovery (as high as 89.4%), and excellent speed (the enrichment can be completed in 10 min). Moreover, this material is also quite effective for enrichment of phosphopeptides from the real sample (drinking milk), showing great potential in the practical application.

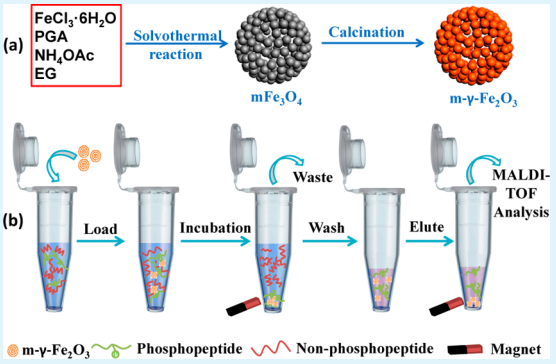

KEYWORDS: *mesoporous γ-Fe_2O_3, nanocrystal clusters, magnetic separation, phosphopeptides, enrichment*

1. INTRODUCTION

Protein reversible phosphorylation is recognized as one of the most biologically relevant post-translational modifications, regulating many essential functions such as cell growth, division, and signal transduction.[1,2] Currently, mass spectrometry (MS) has been demonstrated to be a powerful tool for the analysis of protein phosphorylation; however, even with the rapid development of new instruments, MS analysis of protein phosphorylation is still a challenge due to its highly dynamic nature, low stoichiometry, and the ion suppression effect caused by the abundant coexistence of nonphosphopeptides. Thus, the enrichment of the phosphoproteins/peptides prior to MS analysis is an essential step.

Among the different enrichment strategies, immobilized metal affinity chromatography (IMAC) is the most widely used one. IMAC requires the immobilization of metal ions, such as Fe^{3+}, Ga^{3+}, Zr^{4+}, and Ti^{4+}.[3−6] Recently, metal oxide affinity chromatography (MOAC) based phosphopeptide enrichment methods, including TiO_2[7] and ZrO_2,[8] have grown rapidly because of the high recovery and selectivity. Magnetic nanoparticles have been the focus of intense research, especially in the fields of biological applications.[9−11] Magnetic composite microspheres, merging the fundamentals of IMAC and MOAC with magnetic separation, have been applied for the phosphopeptides enrichment. Magnetic nanoparticles are immobilized with metal ions[12−14] as well as coated with metal oxide.[15,16] Meanwhile, mesoporous metal oxides (TiO_2,[17,18] ZrO_2,[19] HfO_2[20]) have also been developed to provide higher purification efficiency and higher loading capacity due to the large surface areas, together with many active surface sites. In the previous studies, magnetic iron oxide materials were mainly used as the magnetic cores to accelerate the separation; few reports have focused on the phosphopeptides enrichment using bare magnetic iron oxides.[21,22] Mesoporous α-Fe_2O_3 microspheres were first used for the enrichment of phosphopeptides because of their high surface area and the affinity for the phosphopeptides.[23] However, these mesoporous α-Fe_2O_3 microspheres could not be separated by magnet, and the centrifugation is indispensable for separation. As a result, mesoporous ferric oxides with high saturation

Received: September 13, 2012
Accepted: January 7, 2013
Published: January 7, 2013

magnetization are promising substrates for the fast and efficient enrichment of phosphopeptides. However, it is difficult to synthesize magnetic mesoporous ferric oxides, because it is hard to control the hydrolysis and condensation of ferric precursors. To date, mesoporous Fe_2O_3 particles were synthesized mainly through soft templating methods[24−26] or hard templating methods,[27−29] but the process is complicated and the template is relatively difficult to remove. Hence, developing a simple method for preparing magnetic γ-Fe_2O_3 with a mesoporous nature is urgently needed.

One facile method for phosphopeptide enrichment is to coat a porous shell onto the magnetic core for specific interaction with phosphopeptides, but the coating will reduce the magnetic responsiveness and a multistep synthetic route is usually needed. Herein, we present a novel and facile two-in-one strategy to fabricate magnetic mesoporous γ-Fe_2O_3 nanocrystal clusters (m-γ-Fe_2O_3) for selective enrichment of phosphopeptides for the first time. The well designed magnetic m-γ-Fe_2O_3 possess the following features: (1) An excellent magnetic response of m-γ-Fe_2O_3 allows the rapid magnetic separation (less than 5 s), compared with magnetic composite microspheres which have to coat a nonmagnetic layer on the surface of magnetic core; (2) The m-γ-Fe_2O_3 have a large surface area due to the mesopores throughout the magnetic nanocrystal clusters, ensuring the high enrichment capacity of phosphopeptides; (3) The fabrication procedure is quite facile, and the enrichment of phosphopeptides can be completed in a short time (within 10 min); (4) The magnetic m-γ-Fe_2O_3 is, for the first time, applied to enrichment of phosphopeptides from complex peptide mixtures as well as milk, showing high selectivity and sensitivity, demonstrating their potential for practical application.

2. EXPERIMENTAL SECTION

2.1. Chemicals and Reagents. Iron(III) chloride hexahydrate ($FeCl_3{\cdot}6H_2O$), ammonium acetate (NH_4OAc), ethylene glycol (EG) and anhydrous ethanol were purchased from Shanghai Chemical Reagents Company (China) and used as received. Poly(γ-glutamic acid) (PGA) was purchased from Dingshunyin Biotechnology Company (China) and used as received. β-Casein (98%), bovine serum albumin (BSA, 95%), 2,5-dihydroxybenzoic acid (2,5-DHB, 98%), ammonium bicarbonate (ABC, 99.5%), and trypsin (from bovine pancreas, TPCK treated) were purchased from Sigma-Aldrich (St. Louis, MO, USA). Acetonitrile (ACN, 99.9%) and trifluoroacetic acid (TFA, 99.8%) were purchased from Merck (Darmstadt, Germany). Phosphoric acid (85%) and ammonium hydroxide solution (25−28%) were purchased from Shanghai Feida Chemical Reagents Ltd. (Shanghai, China). Drinking milk was purchased from a local grocery store. All these reagents were used as received without further purification. Deionized water (18.4 MΩ cm) used for all experiments was obtained from a Milli-Q system (Millipore, Bedford, MA).

2.2. Preparation of Magnetic Mesoporous Fe_3O_4 Stabilized by PGA. Magnetic mesoporous Fe_3O_4 colloidal nanocrystal clusters (mFe_3O_4) were prepared by a modified solvothermal reaction.[30,31] Typically, 1.350 g of $FeCl_3{\cdot}6H_2O$, 3.854 g of NH_4OAc, and 1.0 g of PGA were dissolved in 70 mL of ethylene glycol. The mixture was stirred vigorously for 1 h at 160 °C to form a homogeneous black solution and then transferred into a Teflon-lined stainless-steel autoclave. The autoclave was heated at 200 °C and maintained for 16 h. Then, it was cooled to room temperature. The resulting mFe_3O_4 were washed several times with ethanol and finally redispersed in ethanol for subsequent use. The mFe_3O_4 were about 200 nm in diameter.

2.3. Preparation of Magnetic Mesoporous γ-Fe_2O_3 by Calcination. Twenty milligrams of mFe_3O_4 was dispersed in 2 mL of ethanol in the combustion boat and then dried for 30 min in the vacuum drying oven until a layer of membrane formed. After that, the boat was put into the muffle furnace, heated slowly to 300 or 500 °C, and calcined for 2 h. Then, it was cooled to room temperature. The resulting mesoporous γ-Fe_2O_3 nanocrystal clusters (m-γ-Fe_2O_3) were washed several times with water and ethanol and then redispersed in ethanol for subsequent use.

2.4. Enrichment of Phosphopeptides Using Mesoporous γ-Fe_2O_3. *2.4.1. Tryptic Digests of Standard Proteins.* β-Casein (1 mg) and BSA (1 mg) were each dissolved in 1 mL of ammonium bicarbonate (25 mM, pH 8.0) and denatured by boiling for 10 min. Protein solutions were then incubated with trypsin with a 1:40 enzyme-to-protein ratio (w/w) for 12 h at 37 °C to produce proteolytic digests, respectively. The tryptic peptide mixtures were stored at −20 °C until further use.

2.4.2. Tryptic Digests of Proteins Extracted from Drinking Milk. Thirty microliters of drinking milk was diluted in ABC (25 mM, 900 μL). This solution was then centrifuged at 16 000 rpm for 15 min, and the supernatant was collected and used for tryptic digestion. After denaturation by boiling for 10 min, the supernatant was incubated with 30 μg of trypsin overnight at 37 °C for proteolysis. The tryptic peptide mixtures were stored at −20 °C until further use.

2.4.3. Enrichment of Phosphopeptides. The obtained m-γ-Fe_2O_3 were first washed with ethanol for three times and then suspended in deionized water (20 mg/mL). Tryptic digests of β-casein and BSA or proteins extracted from drinking milk were dissolved in loading buffer (50% ACN containing 1% TFA, 100 μL), and then, 100 μg m-γ-Fe_2O_3 were added and incubated at room temperature for 10 min. After that, m-γ-Fe_2O_3 with captured phosphopeptides were separated from the mixed solutions using an external magnet. After washing with loading buffer (200 μL) to remove the nonspecifically adsorbed peptides, the trapped phosphopeptides were directly eluted with 5 μL of matrix solution (20 mg/mL DHB in 50% ACN containing 1% H_3PO_4) and 1 μL of mixture was deposited onto the MALDI target for further MS analysis.

2.4.4. MALDI Mass Spectrometry. MALDI-TOF mass spectrometry analysis was performed in positive reflection mode on a 5800 Proteomic Analyzer (Applied Biosystems, Framingham, MA, USA) with a Nd:YAG laser at 355 nm, a repetition rate of 200 Hz, and an acceleration voltage of 20 kV. The range of laser energy was optimized assuring that the absolute intensity of the observed standard peptides was in the range of 12 000−15 000, signal-to-noise ratio (S/N) was over 30, and the laser energy was kept at a constant value for further analysis. External mass calibration was performed using standard peptides from myoglobin digests.

2.5. Characterization. High-resolution transmission electron microscopy (HR-TEM) images were taken on a JEM-2100F transmission electron microscope at an accelerating voltage of 200 kV. Samples dispersed at an appropriate concentration were cast onto a carbon-coated copper grid. Field-emission scanning electron microscopy (FE-SEM) was performed on a Hitachi S-4800 scanning electron microscope at an accelerating voltage of 20 kV. Sample dispersed at an appropriate concentration was cast onto a glass sheet at room temperature and sputter-coated with gold. Powder X-ray diffraction (PXRD) was performed on a Panalytical X'Pert Pro diffraction meter. X-ray photoelectron spectroscopy (XPS) was conducted using an RBD upgraded PHI-5000C (Perkin-Elmer, USA) ESCA system with Mg Kα radiation ($h\nu$ = 1253.6 eV) at 250 W and 14.0 kV with a detection angle at 54°. Raman spectra were recorded on a Renishaw spectrometer (model Invia Reflex) with 632.8 nm laser excitation. The data acquisition time was 10 s, and the peak intensities of the samples were normalized with respect to that of the silicon wafer at 520 cm^{-1}. Nitrogen adsorption−desorption measurements were performed on an ASAP2020 (Micromeritics, USA) accelerated surface area analyzer at 77 K. Before measuring, the samples were degassed in a vacuum at 120 °C for at least 6 h. Magnetic characterization was carried out on a VSM on a Model 6000 physical property measurement system (Quantum, USA) at 300 K. Hydrodynamic diameter (Dh) measurements were conducted by dynamic light scattering (DLS) with a ZEN3600 (Malvern, UK) Nano ZS instrument using He−Ne laser at a wavelength of 632.8 nm.

dx.doi.org/10.1021/am3019806 | ACS Appl. Mater. Interfaces 2013, 5, 614−621

Thermogravimetric analysis (TGA) measurements were performed on a Pyris 1 TGA instrument. All the measurements were taken under a constant flow of nitrogen of 40 mL/min. The temperature was first increased from room temperature to 100 °C and held until constant weight and then increased from 100 to 600 °C at a rate of 20 °C/min.

3. RESULTS AND DISCUSSION

3.1. Preparation of Magnetic Mesoporous γ-Fe_2O_3.

The procedure for synthesis of the mesoporous γ-Fe_2O_3 nanocrystal clusters (m-γ-Fe_2O_3) was schematically illustrated in Scheme 1a. Briefly, the mesoporous Fe_3O_4 nanocrystal clusters (mFe_3O_4) were prepared using a modified solvothermal method, in which PGA acted as stabilizer and resulted in mesopores.[30] Then, the as-prepared mFe_3O_4 were calcined in air to form m-γ-Fe_2O_3 through the oxidation reaction.

Scheme 1. Schematic Illustration of (a) the Synthesis Strategy of m-γ-Fe_2O_3 and (b) the Selective Enrichment Process for Phosphopeptides Using m-γ-Fe_2O_3

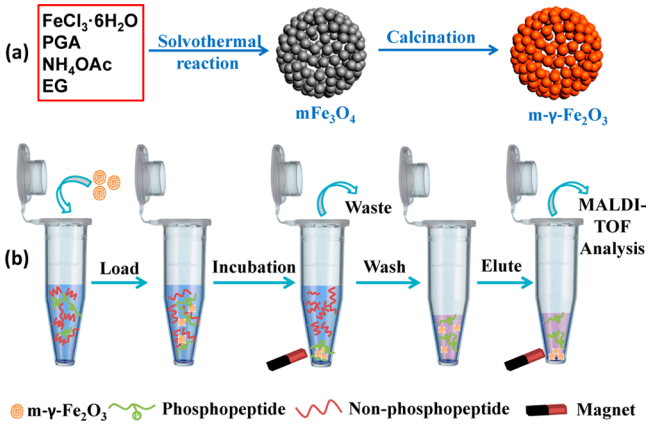

The representative TEM image of the mFe_3O_4 (Figure 1a) reveals that the obtained mFe_3O_4 are structurally loose and have a spherical shape with a mean diameter of about 200 nm. The SEM image shown in Figure 1b clearly demonstrates that the magnetic clusters consist of many small nanocrystals. After calcination in air at 300 or 500 °C, m-γ-Fe_2O_3-300 (calcinated at 300 °C) and m-γ-Fe_2O_3-500 (calcinated at 500 °C) are still composed of many small building nanocrystals, and the previous shapes are well preserved for m-γ-Fe_2O_3-300 (Figure 1c,d). In addition, the magnetic particles changed from black to reddish brown after calcination (Figure S2a, Supporting Information), which indicated the transformation from mFe_3O_4 to m-γ-Fe_2O_3. For m-γ-Fe_2O_3-500, the pores became larger (Figure 1e), which may be due to the rearrangement of nanocrystals. However, when the calcination temperature was increased to 600 °C, hematite (α-Fe_2O_3) particles were produced. Because hematite is the most stable state of iron oxide, stable hematite will be the end product at high temperature, but when the calcination temperature is lower, it tends to become the substable γ-Fe_2O_3.[25] The hydrodynamic diameter and size distribution were determined by dynamic light scattering (DLS). The hydrodynamic diameter (D_h) of mFe_3O_4 is about 280 nm (Figure S1b, Supporting Information), which is quite close to the size measured by TEM. The D_h of m-γ-Fe_2O_3-300 and m-γ-Fe_2O_3-500 changed little after calcination. The polydispersity indexes (PDI) of mFe_3O_4, m-γ-Fe_2O_3-300, and m-γ-Fe_2O_3-500 are 0.117, 0.155, and 0.218, respectively, which indicate that all the particles are nearly uniform.

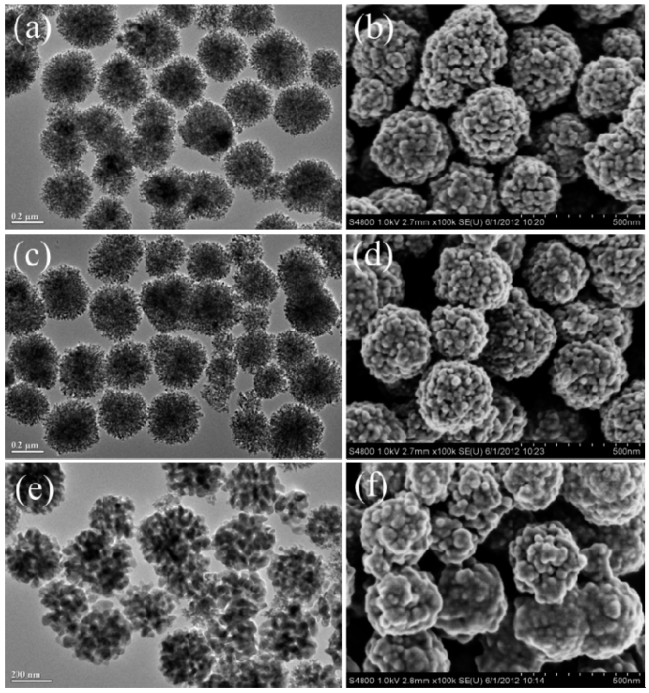

Figure 1. Representative TEM and SEM images of (a, b) mFe_3O_4, (c, d) m-γ-Fe_2O_3-300, and (e, f) m-γ-Fe_2O_3-500. The scale bars for (a, c, e) are 200 nm and for (b, d, f) are 500 nm.

The powder X-ray diffraction (PXRD) patterns of the as-prepared magnetic nanoparticles are shown in Figure 2a. From these PXRD results, we can determine that the resulted particles are γ-Fe_2O_3 or Fe_3O_4 other than α-Fe_2O_3, due to the PXRD pattern of α-Fe_2O_3 being different from Fe_3O_4 or γ-Fe_2O_3 (JCPDS 75-1610 or 25-1402; See Figure S3, Supporting Information).[32] In fact, we cannot distinguish γ-Fe_2O_3 from Fe_3O_4 clearly by PXRD patterns.[33] In order to distinguish them, we further conducted the X-ray photoelectron spectroscopy (XPS) measurement. All the XPS spectra exhibit the peaks at 712.1 and 725.4 eV, which are the characteristic peaks of Fe $2p_{3/2}$ and Fe $2p_{1/2}$ oxidation states (Figure 2b). The curves in Figure 2b (ii) and (iii) have an additional peak at about 720.5 eV, which is the shakeup satellite peak, corresponding to the characteristic peak of Fe^{3+} in Fe_2O_3.[32] Besides, the phase of our materials was also studied by Raman spectroscopy. Raman shifts at 305, 528, and 663 cm^{-1} are the characteristic peaks of Fe_3O_4 and at 352, 500, and 701 cm^{-1} are the characteristic peaks of γ-Fe_2O_3 (Figure S4, Supporting Information).[34] These results mean that the iron oxide phase has transferred from Fe_3O_4 to Fe_2O_3 after calcination. Considering all the results of PXRD, XPS, and Raman spectra, we can conclude that the phase of the magnetic particles after calcination is γ-Fe_2O_3.

The magnetic properties of the particles were determined using vibrating sample magnetometer (VSM). As revealed in the hysteresis loops (Figure 3a), the particles show very strong magnetism at room temperature. For mFe_3O_4, m-γ-Fe_2O_3-300, and m-γ-Fe_2O_3-500 particles, the saturation magnetization (Ms) values are 70.5, 78.8, and 80.5 emu/g, respectively. The Ms values of m-γ-Fe_2O_3 increased compared with mFe_3O_4, revealing the elimination of PGA during the calcination. With such strong magnetism, the magnetic particles can easily be separated from the mixture solution within 5 s using a magnet

dx.doi.org/10.1021/am3019806 | ACS Appl. Mater. Interfaces 2013, 5, 614−621

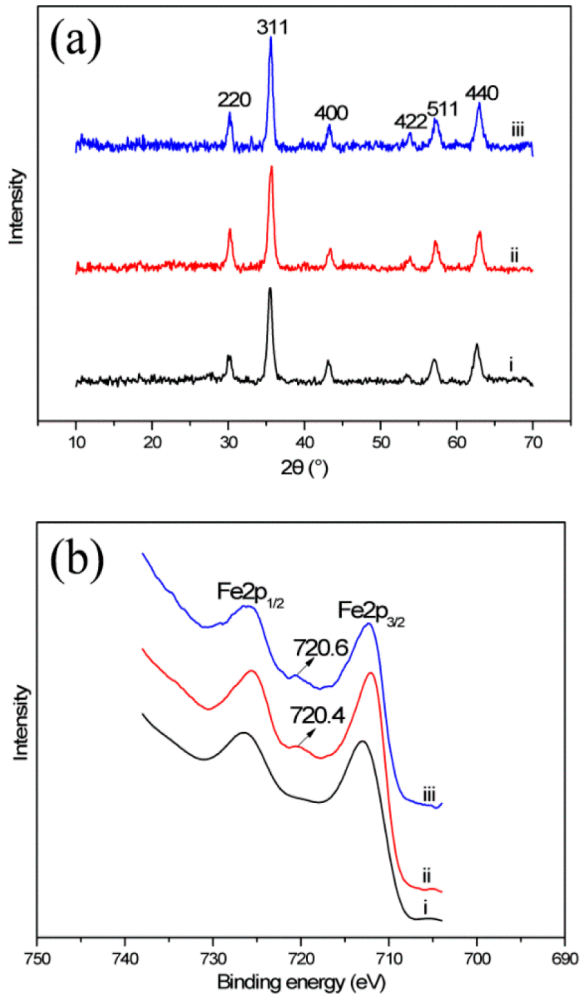

Figure 2. (a) PXRD patterns and (b) XPS spectra of (i) mFe_3O_4, (ii) m-γ-Fe_2O_3-300, and (iii) m-γ-Fe_2O_3-500.

(Figure S2, Supporting Information). This excellent magnetic responsiveness will contribute greatly to rapid and high throughput enrichment and separation of phosphopeptides. The amount of PGA stabilizer in mFe_3O_4 was characterized through thermogravimetric analysis (TGA). The TGA curves of mFe_3O_4, m-γ-Fe_2O_3-300, and m-γ-Fe_2O_3-500 were shown in Figure 3b. The weight loss of (i) mFe_3O_4 is mainly attributed to the amount of PGA, which is finely agreeable with the result gained from VSM. During calcination in air, mFe_3O_4 should gain some weight (about 3%) because of the oxidation of Fe^{2+}. However, the stabilizer PGA in mFe_3O_4 causes a weight loss of about 12%, so the total weight loss was about 9%. For (ii) m-γ-Fe_2O_3-300 and (iii) m-γ-Fe_2O_3-500, there was no weight loss mainly because of the elimination of PGA during the calcination in air. Meanwhile, the component of the material was also proven to be Fe_2O_3, as Fe_3O_4 would show a weight increase due to the oxidation in air.

The mesoporous structure was further characterized by N_2 adsorption/desorption isotherms. The adsorption/desorption isotherms (Figure 4) and the Barrett–Joyner–Halenda (BJH) pore size distribution from the desorption branch (inset in Figure 4) indicate the formation of mesoporous structure among the nanocrystals. The Brunauer–Emmett–Teller (BET) surface area, average pore diameter, and total pore volume are calculated and summarized in Table 1. The

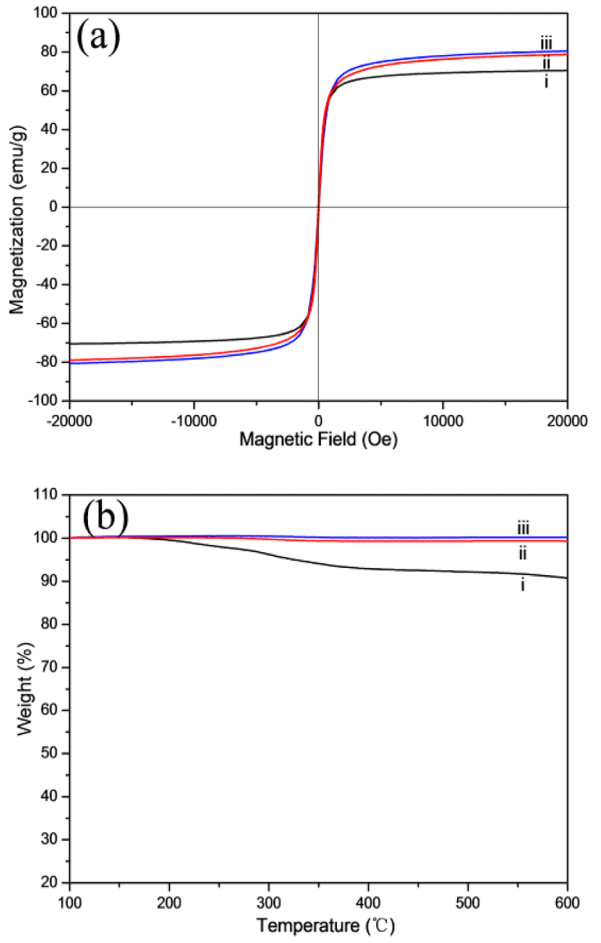

Figure 3. (a) Magnetic hysteresis curves and (b) TGA curves of (i) mFe_3O_4, (ii) m-γ-Fe_2O_3-300, and (iii) m-γ-Fe_2O_3-500.

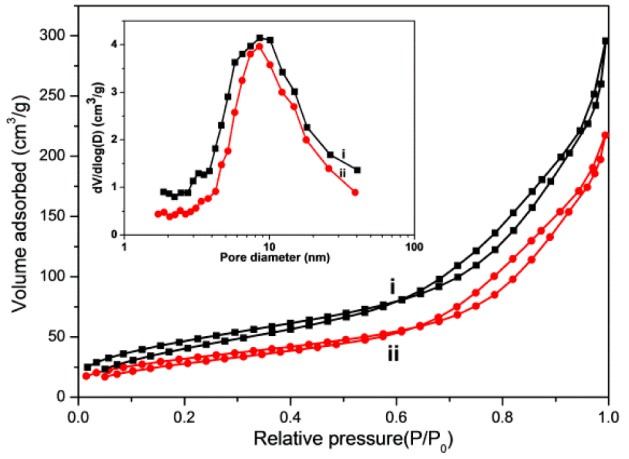

Figure 4. Nitrogen adsorption–desorption isotherms and BJH pore-size distribution curves (inset) for (i) mFe_3O_4 and (ii) m-γ-Fe_2O_3-300.

Table 1. Porous Characteristics of the As-Prepared mFe_3O_4, m-γ-Fe_2O_3-300, and m-γ-Fe_2O_3-500

sample code	surface area (m^2/g)	pore volume (cm^3/g)	pore size (nm)
mFe_3O_4	173.2	0.46	9.5
m-γ-Fe_2O_3-300	117.8	0.34	9.7
m-γ-Fe_2O_3-500	48.9	0.34	25

dx.doi.org/10.1021/am3019806 | ACS Appl. Mater. Interfaces 2013, 5, 614–621

Barrett–Joyner–Halenda (BJH) pore size distribution from the desorption branch shows a peak centered at the mean value of 9.5 nm (mFe_3O_4) and 9.7 nm (m-γ-Fe_2O_3-300), respectively, indicating that the pores mainly arise from the spaces among the nanocrystallites within the magnetic nanocrystal clusters.

3.2. Enrichment of Phosphopeptides Derived from Standard Proteins. Considering the appropriate pore diameter and larger surface area of m-γ-Fe_2O_3-300 compared with m-γ-Fe_2O_3-500, the sample of m-γ-Fe_2O_3-300 was used for the following experiments. In view of the unique characters of the synthesized m-γ-Fe_2O_3-300 and the strong interaction of Fe_2O_3 with the phosphate group, we investigated their applicability in selective enrichment of phosphopeptides using the standard phosphoprotein β-casein as the model. Scheme 1b shows a typical enrichment procedure; 100 ng of β-casein digests were incubated with m-γ-Fe_2O_3-300 in 100 μL of loading buffer (consisting of 50% ACN containing 0.1% TFA) for 10 min. After magnetic separation and thorough washing with the loading buffer, the m-γ-Fe_2O_3-300 particles with trapped phosphopeptides were eluted with 5 μL of matrix solution (20 mg/mL DHB in 50% ACN containing 1% H_3PO_4), and 1 μL of this solution was used for MALDI-TOF MS analysis. For comparison, direct MS analysis of the 20 ng of β-casein digests was also performed (Figure 5a). Without the enrichment procedure, the phosphopeptides signals were severely suppressed by the dominated nonphosphopeptides. However, after selective enrichment with m-γ-Fe_2O_3-300 (Figure 5b), only phosphopeptides signals (listed in Table 1S, Supporting Information) could be distinctly observed (the corresponding dephosphorylated counterparts and doubly charged phosphopeptides were likely formed during the MALDI ionization process) and the nonphosphopeptides were almost eliminated. Additionally, the enrichment experiment using mFe_3O_4 precursor was also performed; the enrichment result (Figure S5, Supporting Information) indicated that the mFe_3O_4 has poor effect on the enrichment of phosphopeptides compared with m-γ-Fe_2O_3-300, which is mainly due to the unclear and nonuniform surface of mFe_3O_4 without calcination.

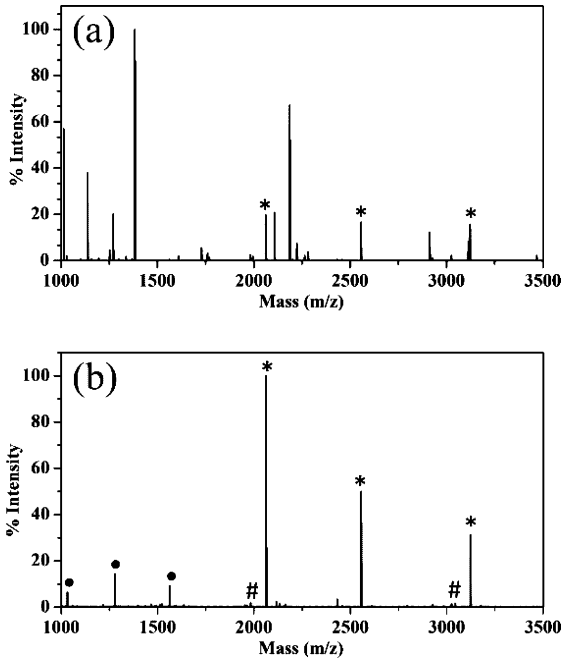

Figure 5. MALDI mass spectra of the tryptic digests of β-casein (a) direct analysis and (b) analysis after enrichment using m-γ-Fe_2O_3-300. "*" indicates phosphopeptides, "#" indicates their dephosphorylated counterparts, and "●" indicates their doubly charged phosphopeptides, respectively.

To further inspect the selectivity of m-γ-Fe_2O_3-300 for the enrichment of phosphopeptides in the presence of a huge amount of nonphosphopeptides, a large amount of tryptic digests of nonphosphorylated protein BSA was added to the tryptic digests of β-casein (the molar ratio of BSA to β-casein is 100:1) in the loading buffer (consisting of 50% ACN containing 1% TFA). As shown in Figure 6a, before enrichment, phosphopeptides were submerged by the high abundance nonphosphopeptides (from the BSA). However, after incubation with m-γ-Fe_2O_3-300 (Figure 6b), the phosphopeptides could be easily detected, without the interference of the nonphosphopeptides. Besides, as a comparison, commercial TiO_2 (Titansphere, 5 μm, GL sciences Inc.) were also used for phosphopeptide enrichment. The results were comparable with that of m-γ-Fe_2O_3 with a clean background in the mass spectrum when only β-casein digests were used as the sample (Figure S6a, Supporting Information). However, when tryptic digest mixtures of β-casein and BSA (with a molar ratio of β-casein to BSA of 1:100) were used as the sample, the efficacy of the enrichment using commercial TiO_2 was inferior, with lower phosphopeptide intensities and nonphosphopeptide peaks dominating the spectrum (Figure S6b, Supporting Information). Besides, the centrifugation is needed when commercial TiO_2 is used for the enrichment which is time-consuming, while fast separation could be easily achieved when our magnetic m-γ-Fe_2O_3-300 is used. The

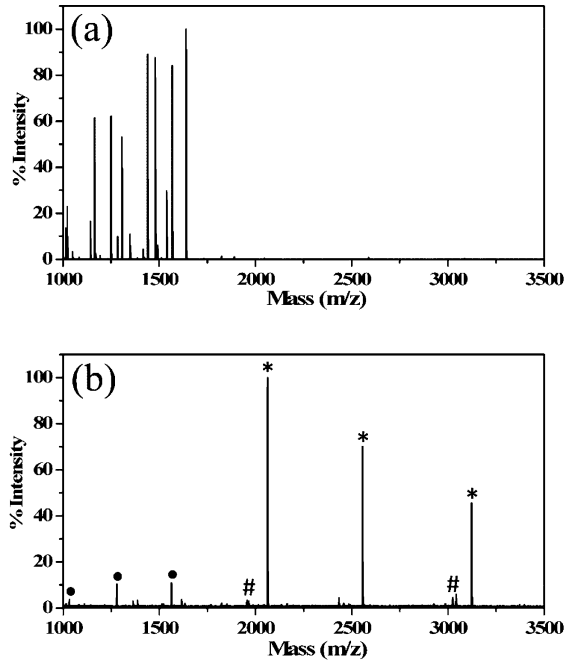

Figure 6. MALDI mass spectra of the tryptic digests mixture of β-casein and BSA (with a molar ratio of β-casein to BSA of 1:100): (a) direct analysis and (b) analysis after enrichment using m-γ-Fe_2O_3-300. "*" indicates phosphopeptides, "#" indicates their dephosphorylated counterparts, and "●" indicates their doubly charged phosphopeptides, respectively.

dx.doi.org/10.1021/am3019806 | ACS Appl. Mater. Interfaces 2013, 5, 614–621

results indicate the high selectivity of m-γ-Fe_2O_3-300 toward phosphopeptides in a short loading time, which benefits from the pure m-γ-Fe_2O_3 without the existence of PGA.

The sensitivity and the postenrichment recovery of m-γ-Fe_2O_3-300 toward phosphopeptides were also investigated. Even when the total amount of β-casein was reduced to only 50 fmol (the concentration was 5×10^{-10} M), all three phosphopeptides of β-casein could still be clearly detected (Figure 7a). The postenrichment recovery was investigated

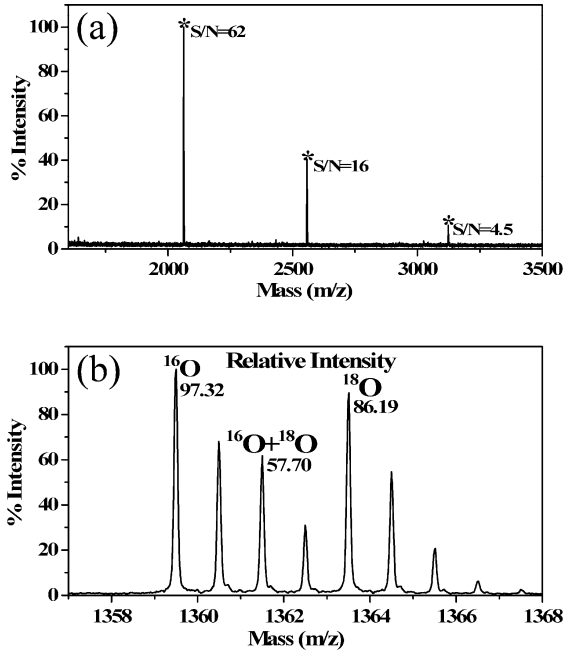

Figure 7. MALDI mass spectrum of (a) tryptic digests of β-casein (0.5 nM, 100 μL), after enrichment using m-γ-Fe_2O_3-300. "*" indicates phosphopeptides; S/N means signal-to-noise ratio. (b) Phosphopeptide EQDSESpQTLDK (a mixture of unlabeled enriched and an equal amount of ^{18}O-labeled unenriched, used as a control).

using the ^{18}O labeling method. A certain amount of standard phosphopeptides (EQDSESpQTLDK) was treated with immobilized trypsin (homemade) in $H_2{}^{18}O$. The natural catalytic activity of trypsin can exchange both C-terminal oxygen atoms with an oxygen atom from water. By performing trypsin digestion in ^{18}O water, both C-termini ^{16}O atoms are replaced with ^{18}O atoms, which produced a 4 Da mass increase of the standard peptides. Another certain amount of standard phosphopeptides were enriched and eluted from m-γ-Fe_2O_3. Then, a theoretically equal amount of the enriched phosphopeptides and labeled phosphopeptides (differing by 4 Da) were mixed and measured by MALDI-MS. According to the relative intensities of the phosphopeptides with different oxygen isotopes that were obtained from the MALDI mass spectrum in Figure 7b and using the equation that was previously reported,[35,36] the recovery of phosphopeptides from the m-γ-Fe_2O_3-300 was calculated to be 89.4%.

3.3. Enrichment of Phosphopeptides from Drinking Milk. The capability of m-γ-Fe_2O_3-300 to selectively trap phosphopeptides was further evaluated using drinking milk as a real sample due to drinking milk containing abundant proteins including phosphoproteins such as α-casein and β-casein. Milk has been widely used as a real complex sample for phosphopeptide enrichment in previous literature.[37,38] In our experiment, the protein concentration of this drinking milk is about 3%, indicated by the milk producer. Figure 8a shows a

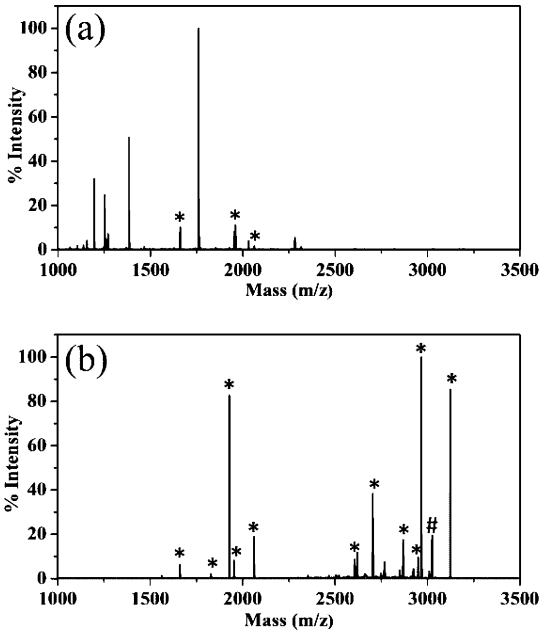

Figure 8. MALDI mass spectra of the tryptic digests of the milk (a) before and (b) after enrichment using m-γ-Fe_2O_3-300. "*" indicates phosphopeptides; "#" indicates the dephosphorylated counterpart.

mass spectrum obtained from direct analysis of 1 μL of tryptic digests of drinking milk; only three weak phosphopeptide peaks appeared before enrichment. However, after extracting with m-γ-Fe_2O_3, more than ten phosphopeptide peaks with relatively high intensity were clearly observed (Figure 8b). For clarity, detected phosphopeptides from the tryptic digests of milk are listed in Table S2, Supporting Information. The results further indicate the potential application of our material in the enrichment of phosphopeptides from real samples.

All of the above results have shown the high selectivity and effectiveness of m-γ-Fe_2O_3-300 in the enrichment of phosphopeptides. The excellent performance is due to the high porosity and large surface area of the mesoporous Fe_2O_3 which can provide more binding sites for phosphopeptides compared with other nanomaterials used for the enrichment of phosphopeptides.[38,39] Compared with the previous reported mesoporous metal oxides,[17,19,20] m-γ-Fe_2O_3 show higher selectivity for phosphopeptides at a low molar ratio of phosphopeptides/nonphosphopeptides (1:100) and lower detection limit (5×10^{-10} M). Moreover, compared with the previous magnetic composite microspheres, the bare m-γ-Fe_2O_3-300 particles show excellent magnetic responsiveness without the reduction in the magnetic properties caused by the thick-coating layer.[18,36] Besides, m-γ-Fe_2O_3 show similar detection limits (fmol level) compared with those employing magnetic particles[15,18] and much better performance than the bare magnetic Fe_3O_4 particles.[21] The inherent capability of convenient enrichment by magnetic separation has an additional advantage as the long-time and high-speed centrifugation needed by nonmagnetic materials often lead to nonspecific entrapment of other peptides.[22] The incorporation of the excellent magnetic property in m-γ-Fe_2O_3 facilitates the rapid and effective enrichment of phosphopeptides.

dx.doi.org/10.1021/am3019806 | ACS Appl. Mater. Interfaces 2013, 5, 614−621

4. CONCLUSION

In summary, we have designed and successfully prepared magnetic mesoporous γ-Fe_2O_3 nanocrystal clusters through a facile method. The well designed m-γ-Fe_2O_3 possessed uniform mesoporous structure as well as high magnetic responsiveness. Then, the magnetic m-γ-Fe_2O_3 particles were applied to rapid enrichment of phosphopeptides, demonstrating high selectivity, excellent sensitivity, and sustainable enrichment recovery to trap phosphopeptides from complex samples within a short time. The experimental results showed that the magnetic mesoporous γ-Fe_2O_3 nanocrystal clusters with only one component could integrate different functions, such as high magnetic responsiveness and many helpful merits on the enrichment of phosphopeptides. This two-in-one strategy has a great potential in practical application. Moreover, considering the easy synthesized processing and low cost, it is convenient to be commercialized.

■ ASSOCIATED CONTENT

Ⓢ Supporting Information

TEM image of a single m-γ-Fe_2O_3-300 particle. DLS plots of m Fe_3O_4, m-γ-Fe_2O_3-300, and m-γ-Fe_2O_3-500. The product mFe_3O_4 and m-γ-Fe_2O_3-300 before and after magnetic separation. The standard PXRD patterns for Fe_3O_4, γ-Fe_2O_3, and α-Fe_2O_3. MALDI mass spectra after enrichment using mFe_3O_4. The Raman spectra of mFe_3O_4 and m-γ-Fe_2O_3-300. MALDI mass spectra after enrichment using commercial TiO_2. List of phosphopeptides detected from β-casein and milk. This material is available free of charge via the Internet at http://pubs.acs.org.

■ AUTHOR INFORMATION

Corresponding Author

*Fax: +86-21-65640293 (C.W.); +86-21-5423-7618 (H.L.). Tel: +86-21-65642385 (C.W.); +86-21-54237618 (H.L.). E-mail: ccwang@fudan.edu.cn (C.W.); luhaojie@fudan.edu.cn (H.L.).

Author Contributions

§Both authors have equal contribution.

Notes

The authors declare no competing financial interest.

■ ACKNOWLEDGMENTS

This work was supported by National Science and Technology Key Project of China (2012CB910602 and 2012AA020204) and National Science Foundation of China (Grant Nos. 21034003, 21025519, 21128001, 21005020, and 51073040).

■ REFERENCES

(1) Ptacek, J.; Devgan, G.; Michaud, G.; Zhu, H.; Zhu, X. W.; Fasolo, J.; Guo, H.; Jona, G.; Breitkreutz, A.; Sopko, R.; McCartney, R. R.; Schmidt, M. C.; Rachidi, N.; Lee, S. J.; Mah, A. S.; Meng, L.; Stark, M. J. R.; Stern, D. F.; Virgilio, C.; De; Tyers, M.; Andrews, M.; Gerstein, M.; Schweitzer, B.; Predki, P. F.; Snyder, M. *Nature* **2005**, *438*, 679–684.

(2) Olsen, J. V.; Blagoev, B.; Gnad, F.; Macek, B.; Kumar, C.; Mortensen, P.; Mann, M. *Cell* **2006**, *127*, 635–648.

(3) Ndassa, Y. M.; Orsi, C.; Marto, J. A.; Chen, S.; Ross, M. M. *J. Proteome Res.* **2006**, *5*, 2789–2799.

(4) Posewitz, M. C.; Tempst, P. *Anal. Chem.* **1999**, *71*, 2883–2892.

(5) Feng, S.; Ye, M. L.; Zhou, H. J.; Jiang, X. G.; Jiang, X. N.; Zou, H. F.; Gong, B. L. *Mol. Cell. Proteomics* **2007**, *6*, 1656–1665.

(6) Hu, L. H; Zhou, H. J.; Li, Y. H.; Sun, S. T.; Guo, S. T.; Ye, M. L.; Tian, X. F; Gu, J. R.; Yang, S. L.; Zou, H. F. *Anal. Chem.* **2009**, *81*, 94–104.

(7) Larsen, M. R.; Thingholm, T. E.; Jensen, O. N.; Roepstorff, P.; Jorgensen, T. J. D. *Mol. Cell. Proteomics* **2005**, *4*, 873–886.

(8) Kweon, H. K.; Hakansson, K. *Anal. Chem.* **2006**, *78*, 1743–1749.

(9) Nata, I. F.; El-Safory, N. S.; Lee, C. K. *ACS Appl. Mater. Interfaces* **2011**, *3*, 3342–3349.

(10) Singh, A.; Dilnawaz, F.; Mewar, S.; Sharma, U.; Jagannathan, N. R. *ACS Appl. Mater. Interfaces* **2011**, *3*, 842–856.

(11) Li, Y.; Ding, M. J.; Wang, S.; Wang, R. Y.; Wu, X. L.; Wen, T. T.; Yuan, L. H.; Dai, P.; Lin, Y. H.; Zhou, X. M. *ACS Appl. Mater. Interfaces* **2011**, *3*, 3308–3315.

(12) Tan, F.; Zhang, Y. J.; Mi, W.; Wang, J. L.; Wei, J. Y.; Cai, Y.; Qian, X. H. *J. Proteome Res.* **2008**, *7*, 1078–1087.

(13) Zhao, L.; Wu, R. A.; Han, G. H.; Zhou, H. J.; Ren, L. B.; Tian, R. J.; Zou, H. F. *J. Am. Soc. Mass Spectrom.* **2008**, *19*, 1176–1186.

(14) Li, Y. C.; Lin, Y. S.; Tsai, P. J.; Chen, C. T.; Chen, W. Y.; Chen, Y. C. *Anal. Chem.* **2007**, *79*, 7519–7525.

(15) Chen, C. T.; Chen, Y. C. *Anal. Chem.* **2005**, *77*, 5912–5919.

(16) Li, Y.; Leng, T. H.; Lin, H. Q.; Deng, H. Q.; Xu, X. Q.; Yao, N.; Yang, P. Y.; Zhang, X. M. *J. Proteome Res.* **2007**, *6*, 4498–4510.

(17) Tang, J.; Yin, P.; Lu, X. H.; Qi, D. W.; Mao, Y.; Deng, C. H.; Yang, P. Y.; Zhang, X. M. *J. Chromatogr., A* **2010**, *1217*, 2197–2205.

(18) Ma, W. F.; Zhang, Y.; Li, L. L.; You, L. J.; Zhang, P.; Zhang, Y. T.; Li, J. M.; Yu, M.; Guo, J.; Lu, H. J; Wang, C. C. *ACS Nano* **2012**, *6*, 3179–3188.

(19) Nelson, C. A.; Szczech, J. R.; Xu, J. R.; Lawrence, M. J.; Jin, M. J.; Ge, Y. *Chem. Commun.* **2009**, *43*, 6607–6609.

(20) Nelson, C. A.; Szczech, J. R.; Dooley, C. J.; Xu, C. J.; Lawrence, M. J.; Zhu, H. Y.; Jin, S.; Ge, Y. *Anal. Chem.* **2010**, *82*, 7193–7201.

(21) Lee, A.; Yang, H. J.; Lim, E. S.; Kim, J. K.; Kim, Y. S. *Rapid Commun. Mass Spectrom.* **2008**, *22*, 2561–2564.

(22) Huang, Y.; Shi, Q. H.; Tsung, C. H.; Gunawardena, H. P.; Xie, L.; Yu, Y. B.; Liang, Y. B.; Yang, P. Y.; Stucky, G. D.; Chen, X. *Anal. Biochem.* **2011**, *408*, 19–31.

(23) Han, L.; Shan, Z.; Chen, D. H.; Yu, X. J.; Yang, P. Y.; Tu, B.; Zhao, D. Y. *J. Colloid Interface Sci.* **2008**, *318*, 315–321.

(24) Malik, A. S.; Duncan, M. J.; Bruce, G. *J. Mater. Chem.* **2003**, *13*, 2123–2126.

(25) Long, J. W.; Logan, M. S.; Rhodes, C. P.; Carpenter, E. E.; Stroud, R. M.; Rolison, D. R. *J. Am. Chem. Soc.* **2004**, *126*, 16879–16889.

(26) Jiao, F.; Bruce, P. G. *Angew. Chem., Int. Ed.* **2004**, *116*, 6084–6087.

(27) Tian, B. Z.; Liu, B. Z.; Solovyov, L. A.; Liu, Z.; Yang, H. F.; Zhang, Z. D.; Xie, S. H.; Zhang, F. Q.; Tu, B.; Yu, C. Z.; Terasaki, O.; Zhao, D. Y. *J. Am. Chem. Soc.* **2004**, *126*, 865–875.

(28) Jiao, F.; Harrison, A.; Jumas, J. C.; Chadwick, A. V.; Kockelmann, W.; Bruce, P. G. *J. Am. Chem. Soc.* **2006**, *128*, 5468–5474.

(29) Kong, A. G.; Wang, H. W.; Li, J.; Shan, Y. K. *Mater. Lett.* **2008**, *62*, 943–945.

(30) Luo, B.; Xu, S.; Luo, A.; Wang, W. R.; Wang, S. L.; Guo, J.; Lin, Y.; Zhao, D. Y.; Wang, C. C. *ACS Nano* **2011**, *5*, 1428–1435.

(31) Ge, J. P.; Hu, Y. X.; Biasini, M.; Beyermann, W. P.; Yin, Y. D. *Angew. Chem., Int. Ed.* **2007**, *46*, 4342–4345.

(32) Wu, G.; Tan, G.; Li, G. Y.; Hu, C. W. *J. Alloys Compd.* **2010**, *504*, 371–376.

(33) Jiao, F.; Jumas, J. C.; Womes, M.; Chadwick, A. V.; Harrison, A.; Bruce, P. G. *J. Am. Chem. Soc.* **2006**, *128*, 12905–12909.

(34) deFaria, D. L. A.; Silva, S. V.; deOliveira, M. T. *J. Raman Spectrosc.* **1997**, *28*, 873–878.

(35) Yao, D.; Freas, A.; Ramirez, J.; Demirev, P. A.; Fenselau, C. *Anal. Chem.* **2001**, *73*, 2836–2842.

(36) Liu, Z.; Cao, J.; He, Y. F.; Qiao, L.; Xu, C. J.; Lu, H. J.; Yang, P. Y. *J. Proteome Res.* **2010**, *9*, 227–236.

(37) Li, Y. C.; Lin, Y. S.; Tsai, P. J.; Chen, C. T.; Chen, W. Y.; Chen, Y. C. *Anal. Chem.* **2007**, *79*, 7519–7525.

(38) Cheng, G.; Zhang, J. L.; Liu, Y. L.; Sun, D. H.; Ni, J. Z. *Chem. Commun.* **2011**, *47*, 5732−5734.
(39) Sturm, M.; Leitner, A.; Smatt, J. H.; Linden, J. H.; Lindner, W. *Adv. Funct. Mater.* **2008**, *18*, 2381−2389.